Materials Advances

PAPER

Check for updates

Programming fibril alignment and mechanical response in reconstituted collagen fibers using reagent-free biomimetic energetic electron crosslinking†

Anastassiya Bublikova,‡[ab] Friedrich Schütte [ID] ‡*[ab] and Stefan G. Mayr*[ab]

Due to its abundance in vertebrates, including humans, collagen is deemed to be a highly attractive bioderived material which bears large potential for cutting-edge applications in a variety of biomedical fields, including scaffolds, implantology, artificial organs, regenerative medicine and mechanobiology. Depending on structure, including hierarchical fibril alignment and crosslinking, *in vivo* collagen assemblies are characterized by Young's moduli ranging from some kPa to GPa. When heading for biomimicry of scaffolds and implants based on reconstituted collagen, control of mechanical response by fibril alignment and biomimetic crosslinking constitute central challenges. Within this work we demonstrate, that energetic electrons are a promising tool to permanently imprint prestrain-induced alignment of collagen fibrils within macroscopic collagen fibers by introduction of biomimetic crosslinks, resulting in elastic properties bridging orders of magnitude.

1 Introduction

Collagen is a versatile biomaterial that has tremendous potential in scientific, applied, and biomedical fields. It is biocompatible and biodegradable showing a high suitability for applications in areas of bio-engineering and regenerative medicine[1] as tissue replacement and in cell culture.[2–6] Collagen is a structural protein that is found in vertebrates, including connective tissues of mammals and humans, in the form of fibers.[7,8] Up to date, 29 types of collagen have been identified, of which type I, II, III, IV, and IX are the most common in humans.[9,10] Collagen type I is the most abundant protein in the human body and plays a critical role in providing structural support and strength to tissues such as skin, bone, cartilage, and tendons.[7,11,12] In living organisms, collagen fibers are typically organized in different orientations depending on the tissue type, which plays an important role in the mechanical, physiological and biochemical functions.[8] Collagen networks display highly nonlinear mechanics and stiffen significantly due to an internal and external strain increase.[13–15] In addition, they are also viscoelastic: they partially store elastic energy and

partially relax internal stress through dissipative processes.[16] All of these properties are delicately influenced by the structure of the networks, by the molecular interactions between monomers, and by the addition of covalent cross-links.[14]

As it is relatively easy to isolate from a variety of tissue sources, such as bovine,[17] fish[18] and rodent,[19] and can be produced as a recombinant human protein,[20] researchers are exploring the use of reconstituted collagen for a range of applications, including drug delivery[21] and wound healing.[18,22] Collagen-based drug delivery systems can protect drugs from degradation and the use of different cross-linking agents can also affect the release rate of drugs. Collagen-based dressings have been shown to promote wound healing by providing a moist wound environment and promoting the growth of new tissue. Collagen has been also extensively studied as a scaffold material for tissue engineering, with many examples of collagen-based biomaterials emerging in recent years.[23,24] One major challenge is the development of biomaterials that can support the growth and function of cells. Collagen-based scaffolds have been shown to promote cell attachment, proliferation, and differentiation. Collagen fibers can be modified to improve their mechanical properties, stability and biological performance by adding cross-links.[25,26] Chemical cross-linking using glutaraldehyde is common and widely used to tailor thermal and mechanical properties of a variety of biomaterials including collagen.[27–29] However, it is often associated with cytotoxicity which interfere drastically with biocompatibility.[30,31] Treatment with energetic electrons, in contrast, is a reagent-free, biomimetic approach eliminating particularly the potential toxicity of chemical cross-linkers[32] and allows for

a Division of Surface Physics, Department of Physics and Earth System Sciences, University of Leipzig, Linnéstr. 5, 04103 Leipzig, Germany.
E-mail: friedrich.schuette@uni-leipzig.de, stefan.mayr@iom-leipzig.de
b Leibniz Institute of Surface Engineering (IOM), Permoserstr. 15, 04318 Leipzig, Germany
† Electronic supplementary information (ESI) available. See DOI: https://doi.org/10.1039/d3ma01111a
‡ These authors contributed equally to this work.

spatially resolved insertion of crosslinks.[33] Previous studies have already demonstrated that electron treated hydrogels[25,34] have been proven to have an influence on cellular morphology while also being non-cytotoxic which makes them even more suitable in the fields of mechanobiology and regenerative medicine.[1]

While there are numerous methods available for forming collagen scaffolds from isolated collagen, it can be difficult to control collagen fibril alignment. While various forms of physical manipulation including fluid shear[35,36] and electromagnetic fields[36,37] have been explored to improve collagen fibril alignment, exposure to strain[38,39] before cross-linking is used in this work to produce reconstituted collagen type I fibers and increase fibril alignment. The collagen fibers are stretched using a tensile testing machine prior to being crosslinked with high energy electron irradiation at different doses in order to tailor and imprint their structural alignment and mechanical properties. This allows the mechanical properties to be simultaneously adjusted on two parameters, which means that a higher degree of accuracy in the mechanical response and mechanical anisotropy can be expected for custom-made scaffolds.

To establish structure–property relationships between fiber alignment and mechanics, polarized light microscopy (PLM)[40] was found to be useful in analyzing changes in polymer structures parallel to mechanical tests. In this paper we use classical cross-polarized light microscopy to image the structure of prestrained and electron treated collagen fibers.

We present approaches to synthesize and cross-link prestrained collagen fibers extracted from rat tail tendons. We show that modification of the mechanical response can be achieved not only by using high-energy electrons, but also by aligning the internal fibril structure by prestraining and fixing it in the aforementioned electron beam treatment. The obtained elastic, viscoelastic and plastic properties of prepared non-prestrained collagen fibers are compared with those of irradiated fibers with respect to the electron irradiation dose as well as the degree of mechanical prestrain before application of energetic electrons. Afterwards, fibers were imaged using cross-polarized light microscopy to reveal and compare their modified structure.

2 Materials and methods

2.1 Collagen sample preparation

Collagen fiber samples were produced according to the work of Y. Kato et al.[19] using chemicals listed in Table 1. Firstly, fiber formation buffer (FFB) is prepared before collagen fiber synthesis consisting of: distilled water (400 ml), 135 mM sodium chloride (2.75 g), 30 mM TES (3.16 g), 30 mM sodium phosphate dibasic (1.7 g).

Using a hypodermic needle, collagen type I extracted from rat tail (5 ml) is slowly loaded into a syringe after centrifuging at 1000 rpm to extract air bubbles of collagen. The polytetrafluoroethylene (PTFE) connector tube is attached to this collagen-filled syringe and the syringe is loaded onto a syringe pump. The end of the connector tube has to be entirely submerged in the fiber formation buffer (FFB), outlined above. This FFB is poured into a large petri dish and placed onto a hot plate with a magnetic stirrer and heated to approximately 36 °C (see Fig. S1, ESI†). The pump infusion rate of the syringe pump is set to 0.2 ml min^{-1} and fibers start forming as soon as syringe pump is turned on and collagen is extruded into the FFB. This extruded collagen needs to be cut with clean sharp scissors every 20 seconds in order to obtain individual fibers of length of approximately 10 cm.

The fibers should remain in the FFB for at least 45 minutes in order to facilitate the polymerisation process. They are then washed in a series of 4 baths at room temperature, each bath lasting 60 minutes. Each subsequent bath decreases concentration of isopropyl alcohol, starting with 100% isopropyl alcohol and ending with 100% dH$_2$O. After the last bath in distilled water, the fibers are hung to dry overnight at room temperature. The samples are stored dry at room temperature until use.

Collagen fibers are stretched in the Zwick-Roell tensile testing machine before irradiation with 0%, 25% or 60% of their original length. This process is referred to as "prestraining" throughout this paper. The fibers are glued onto a sample holder which is a frame of transparency paper and has a fixed gauge length (initial length of specimen), 3–4 dried fibers are glued at both ends by cyanoacrylate adhesive to a sample holder. The samples are then submerged in a bath with dH$_2$O to swell for at least 30 minutes. The wet fibers attached to the sample holder are then clamped in the tensile testing machine and the sides of the sample are cut to allow the fibers to be stretched. The upper clamp then moves upwards at a steady speed until the samples reach the desired extension. When the clamp stops moving, without removing the sample holder from the clamp, a piece of Styrofoam is glued to either side of the sample holder in order to fix this new fiber length. These samples are then stored dry at room temperature until irradiation.

Table 1 Table of chemicals

Chemical name	Concentration/lab code
Collagen	Collagen Type I, Rat Tail, Cat. No.: 50205, pH 2–3 (ibidi GmbH, Germany)
Buffer	Sodium chloride NaCl, $M = 58.44$ g mol^{-1}, S7653 (Sigma-Aldrich, Germany)
	TES $C_6H_{15}NO_6S$, $M = 229.25$ g mol^{-1}, T1375 (Sigma-Aldrich, Germany)
	Sodium phosphate dibasic Na_2HPO_4, $M = 141.96$ g mol^{-1}, S3264 (Sigma-Aldrich, Germany)
Distilled water	dH_2O, $M = 18.02$ g mol^{-1}
Isopropyl alcohol	C_3H_8O, $M = 60.10$ g mol^{-1}, 278 475 (Sigma-Aldrich, Germany)
Sodium hydroxide	NaOH, $M = 40.00$ g mol^{-1}, 72 068 (Sigma-Aldrich, Germany)

2.2 Electron irradiation

A 10 MeV linear accelerator (MB10-30MP; Mevex, Ontario, Canada) was used to irradiate collagen fibers. The precise device used is located in the Leibniz-Institute for Surface Modification e.V. Leipzig. The moving stage moves with a 180 HZ frequency rate, electron pulse of 8 μs long was used and the scanning horn scans the electron beam with a frequency of 3 Hz, similarly to Riedel et al.[25] Irradiation is done in steps of 5 kGy in accordance to Wisotzki et al.,[34] regardless of the final desired irradiation dose, with a rest period of 2–3 minutes between each step to prevent overheating and damaging of the samples. As a result, the total time to irradiate the samples takes approximately an hour, depending on the final irradiation dose. The irradiation doses are measured using graphite dosimeter having an uncertainty of 10%. The samples were irradiated up to 50 kGy in an inert plastic sample holder filled with distilled water.

2.3 Tensile testing

A zwickiLine tensile testing machine (type Z0.5 TS, art. no. 058992, ZwickRoell GmbH & Co. KG, Germany) was used for prestraining and tensile testing of the collagen fibers. The built-in force sensor (type Xforce HP, art. no. 063924, ZwickRoell GmbH & Co. KG, Germany) is calibrated to 0.4% of the nominal force (i.e. max 0.02 N). The computer software testXpert III sets the parameters and collects the force data for the stress–strain curves at a sampling rate of 200 Hz. All tensile tests were performed strain controlled in fully hydrated conditions. Stress is obtained from the measured force acting in the direction parallel to the fiber ($\sigma = F/A_0$ where $A_0 = \pi r_0^2$ and r_0 is the initial radius) with a uniform loading rate of 1.5 mm min^{-1}.

For tensile testing, sample holders are prepared consisting of a frame of transparency paper which is cut with a fixed gauge length of 2 mm. This allowed a strain to be determined based on the standardized original sample length and the displacement measured with the calibrated ZwickRoell (type Z0.5 TS, art. no. 058992, ZwickRoell GmbH & Co. KG, Germany) force testing system. The fibers are glued with cyanoacrylate adhesive to a sample holder. The samples swell in a water bath for at least 2 hours before tensile testing. The sample is then clamped vertically inside a water bath in the tensile testing machine (shown in Fig. S2 and S3, ESI†). Each side of the sample holder is then cut to allow the collagen fiber to be stretched. The bottom clamp is stationary fixing the sample in place while the upper one moves, stretching the sample vertically. The light microscope set up behind the water bath allows real-time recording of the sample being measured.

2.4 Polarization microscopy

Polarized light microscopy was used to image the collagen fiber structure. The microscope Leica DM2700M (LeicaMicrosystems GmbH, Wetzlar, Germany) was configured to polarisation mode in accordance with the manual.[41] The polariser and analyzer are initially set at 0° with respect to each other to obtain unpolarized images of the samples. Analyzer is then rotated 90° with respect to the polarizer, in this cross-orientation of the polarizers, the birefrigent sample appears bright on a dark background. The samples are imaged in a fully hydrated state by letting them swell in a water bath of dH$_2$O for approximately 2 hours and more water being applied to the fiber during the measurement if needed. The light source used in the microscope is a white light high-power LED. Different objectives with increasing magnification are used to image the samples in greater detail (5×, 10×, 20×, 40×, 63×).

2.5 Image and data analysis

The light microscope used during the tensile measurement is DinoLite AM7915MZT (AnMo Electronics Corporation, Taipei, Taiwan) with the DinoCapture 2.0 software. The images obtained from the polarization microscope were scaled to size using imageJ (version v1.53t) software. The data obtained from the tensile testing machine was analyzed using Python 3.6.15 code, analysis and fitting were done using the libraries NumPy, SciPy and Pandas, while the plotting is done using MatPlotLib.

3 Results

3.1 Uniaxial mechanical characterization

Tensile tests were performed to determine viscoelastic behaviour of fully hydrated unirradiated non-prestrained (see Fig. S4, ESI†) and irradiated prestrained collagen fibers, respectively. In Fig. 1 for each electron dose D (5, 10, 25, 50 kGy, respectively) four stress–strain curves are shown, as-extruded, irradiated non-prestrained, irradiated prestrained 25% and irradiated prestrained 60%, respectively, employing the engineering stress and strain definitions. Regarding the qualitative shape of the curves, first it is interesting to note that by introduction of covalent crosslinks, energetic electron treatment prevents occurrence of ductile necking behavior, which is prevalent only in as-extruded samples. With both, higher dose and prestrain, fracture strain decreases while ultimate tensile strength (UTS) increases. The higher the dose, the stiffer the fiber becomes, thus the fracture strain decreases with each higher dose (see Table S1, ESI†). For as-extruded and samples exposed to doses of 10 kGy and higher, increases of UTS from 0.16 MPa to 0.77 MPa and higher, respectively can be observed. If prestrains $\varepsilon_{pre} = 25\%$ and $\varepsilon_{pre} = 60\%$ are applied, UTS at 50 kGy are 1.47 MPa and 3.50 MPa, respectively.

The mechanical properties of cross-linked collagen fibers were determined by cyclically loading in loops of 10 cycles each, resulting in four loops with increasing maximum strains of 0.02, 0.04, 0.08, and 0.16, respectively. Cyclic stress–strain tests were mainly performed in the low-strain region, revealing a nonlinear elastic response indicating a central role of induced crosslinks for mechanical stability. For each loop the distribution of the differential Young's moduli $K = d\sigma/d\varepsilon$[42] was investigated at constant loading rate of 1.5 mm min^{-1} at frequencies of $f_{2\%} = 0.313$ Hz, $f_{4\%} = 0.157$ Hz, $f_{8\%} = 0.078$ Hz, $f_{16\%} = 0.039$ Hz, $f_{32\%} = 0.020$ Hz, respectively, as determined by the maximum deformation strains due to constant deformation rates (see Table S1, ESI†). The resulting stress–strain curves were smoothed with a spline fit
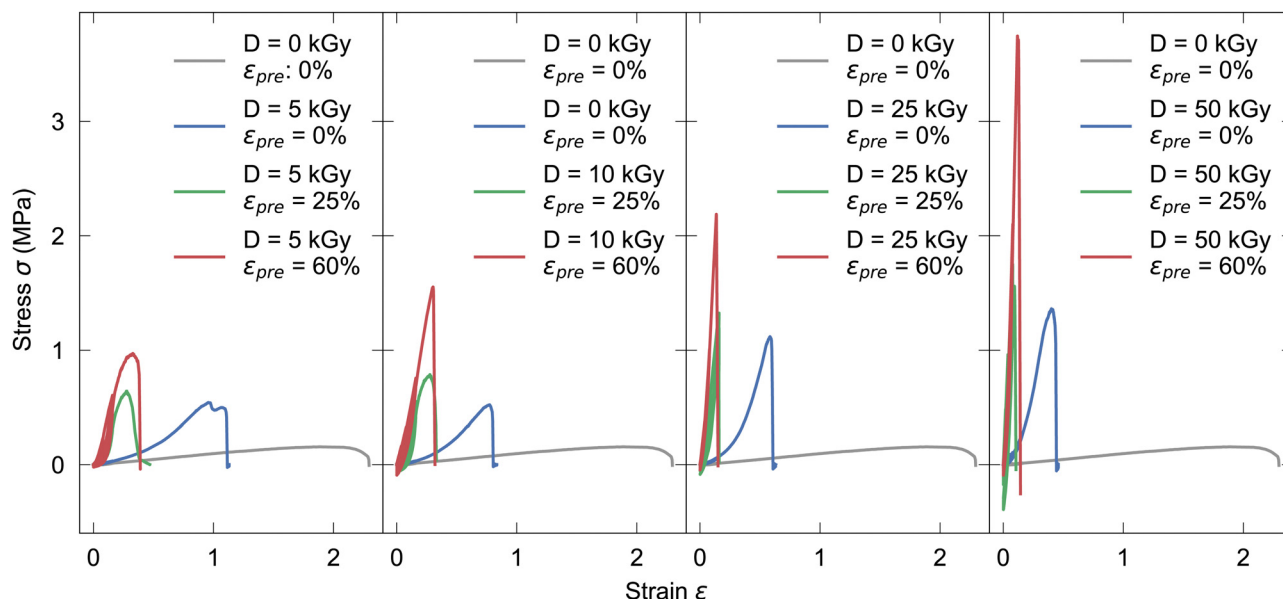
Fig. 1 Exemplary tensile tests with 0%, 25%, 60% prestrain for increasing irradiation doses of 5, 10, 25 and 50 kGy from left to right, compared to unirradiated samples.

in python,[43] whereby K was defined as the stress gradient σ divided by the strain gradient ε. The differential moduli were calculated solely for extension, not for compressions in the respective loops. Depending on the prestrain, *i.e.* 0%, 25%, 60%, results are shown in Fig. 2 for the respective irradiation doses; they basically not only show an increasing Young's modulus with prestrain and dose, but also non-linearity, as reflected in the broadening of the distribution (see also Fig. S5–S7, ESI†).

Since the cyclic force tests show a hysteretic response, energy dissipation is analyzed *via*

$$W = \int_{t_1}^{t_2} \vec{F}(\vec{s}(t)) \cdot \frac{\mathrm{d}\vec{s}}{\mathrm{d}t} \mathrm{d}t \qquad (1)$$

where t_1 is the start time and t_2 the end time of the stress–strain measurement. The total distance traversed by the moving head of the force measurement system at the corresponding time is the displacement $\vec{s}(t)$. A higher irradiation dose does not have a particularly large effect on dissipation (also Fig. S8, ESI†). For a prestrain, however, it can be observed that the energy dissipation decreases dramatically. In fact, in Fig. 3, for cycles 20 and above, the energy dissipation is at least an order of magnitude higher for as-extruded samples when compared with prestrained samples. A distinction must be made between low-strain regions (up to cycle 20) in which almost no energy dissipation appears, and regions above this where the first relaxation effects can already be observed (*cf.* Fig. 3).
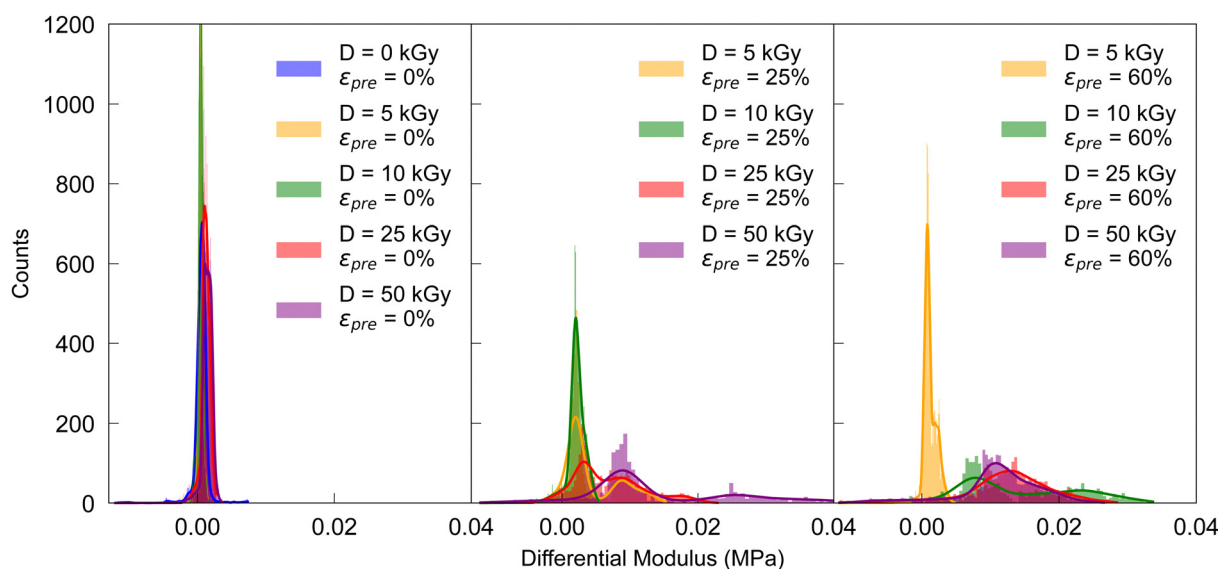

Fig. 2 Distribution of differential moduli in the loop up to 4% peak strain for increasing prestrains in cyclic stress–strain curves.
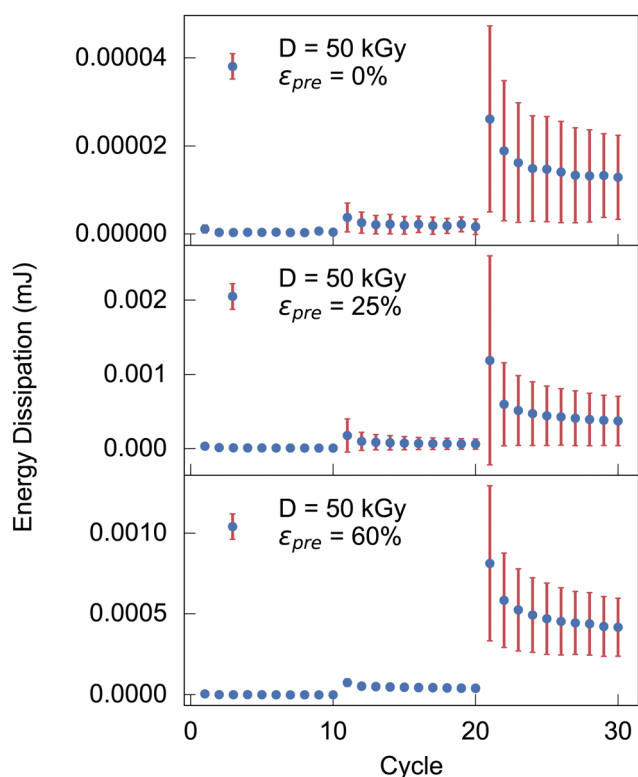
Fig. 3 Energy dissipation during cyclic measurements with a peak strains of 0.02, 0.04, 0.08 for the cycle 1 to 10, 11 to 20, 21 to 30, respectively, for increasing prestrains.

The relaxation behaviour of glassy complex systems can be modeled by introducing an additional stretch parameter[44] to an exponentially decaying function. The stretched exponential is defined as

$$\sigma_k(t) = \sigma_0 \cdot \exp\left[-\left(\frac{t}{\tau}\right)^{\beta}\right] \qquad (2)$$

referred as the Kohlrausch–Williams–Watts (KWW) function, in this case with $\sigma_k(t)$ as time dependent stress, σ_0 as initial value of the stress and $0 < \beta \leq 1$ as stretch parameter. The stress in relaxation curves was transformed from the measured forces, the time scale remained identical. Relaxation covering stretched exponential fits were performed with the curve_fit function from the python[43] scipy library. The KWW function (2) was slightly adapted for the fit. An additional offset t_0 was added to capture relaxation effects occuring before starting the measurements. In order to cover the stress range of the measurement, an offset σ_{off} is added; thus the prefactor σ_0, originally initial stress value, must be adjusted.

$$\sigma'_k(t) = \sigma'_0 \cdot \exp\left[-\left(\frac{t + t_0}{\tau}\right)^{\beta}\right] + \sigma_{\text{off}} \qquad (3)$$

To reduce fit parameters and to include the offset σ_{off} on the stress axis, σ'_0 is written as

$$\sigma'_0 = (\sigma_0 - \sigma_{\text{off}}) \exp\left[\left(\frac{t_0}{\tau}\right)^{\beta}\right] \qquad (4)$$

with

$$\sigma_0 = \sigma'_k(t = 0). \qquad (5)$$

The fit parameters τ, β, σ_{off}, t_0 have been determined using as well eqn (3) as eqn (4) and constraints resulting from the data.

For the fitting procedure, the measurement data in the 4th loop from the cyclic stress–strain tests were averaged. The stretched exponential fit described above was then applied to the maximum mean values of the respective cycles. The values for the stretching exponent is in our study in the range of $0.2 < \beta < 1$, whereby β decreases with increasing dose, *viz.* cross-linking density (see Fig. 4 0 kGy and 5 kGy). The results of the stretched exponential fits in the relaxation tests are approximately consistent with other studies.[45]

3.2 Characterization of fiber alignment using polarized light microscopy

The samples were imaged under cross-polarized light and were rotated on the rotating plate 10° at a time (starting at 0° with sample being parallel to *x*-axis) in order to investigate further the inner alignment of the fibers. Brightness of the microscope's light source was lowered significantly for imaging as in the section above the samples were imaged at extinction (0°), as is clear from the images below. The same brightness as used in the imaging above results in samples being too bright when imaged at 45°. Only images at 0° and 45° are shown here because they provide the extinction and brightest position of the fibers, respectively.

All samples in the images below appear brightest at 45° and dimmest at 0° and 90°. The non-prestrained and unirradiated sample is the brightest out of all samples at 45°, appearing mostly white. At 0° the sample appears blue and is still clearly visible. When unirradiated sample is stretched a portion of the light appears to be absorbed leaving the sample at extinction to appear orange on the outer edges at 0° and entirely at 45°.

When irradiated but still non-prestrained, the sample looks similar to the unirradiated non-prestrained sample, but dimmer at all angles. This is similar to what is seen for the unirradiated and irradiated non-prestrained samples shown in Fig. 5. When stretched, similar to the unirradiated sample, it appears orange but now at 45° while being completely extinct at 0°. Prestrained irradiated samples show similar colours to Fig. 5 at 45° and are completely extinct at 0°.

The image data from the polarization microscopy were evaluated *via* the intensity histograms (see Fig. S14, ESI†) of the individual red, green and blue channels (RGB) in order to assign potential effects of irradiation or induced stresses. Polar plots in Fig. 6 show intensity dependence for $0° \leq \alpha \leq 180°$.

4 Discussion

In the following, we aim to discuss the relation of collagen network properties and mechanical response. We start by first noting that our extruded collagen fibers largely consist of
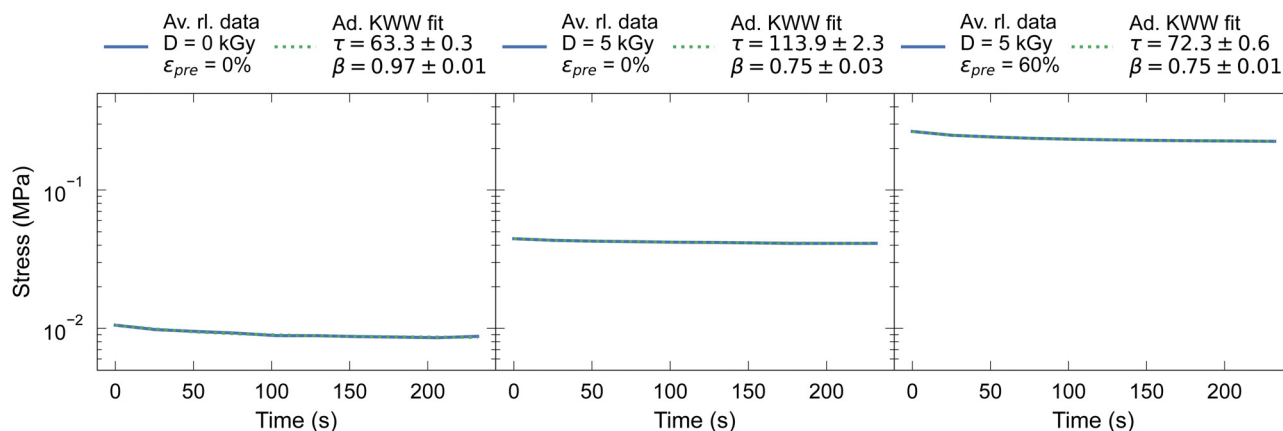
Fig. 4 Averaged relaxation curves (Av. rl. data) with fitted data using an adapted KWW function (Ad. KWW fit) for prestrained crosslinked samples and unmodified reference samples.

isotropic network structure, as confirmed by our present polarized light microscopy measurements (as-extruded fibers in absence of prestrain largely reveal zero transmittance when rotated between two crossed linear polarizers), as well as previous ESEM (environmental scanning electron microscopy) measurements.[46] Energetic electron treatment of such isotropic networks results in dramatically increasing elastic moduli as *e.g.* reflected by the maximum Young's modulus, which increases *e.g.* by 1.5 orders of magnitude from 0.1 to 5 MPa upon exposure to an electron dose of 50 kGy. This is accompanied by a change of fracture mode from ductile to brittle; accordingly UTS and fracture strain increase (0.18 → 1.2 MPa) and decrease (2.4 → 0.5) by an order of magnitude and more, respectively. While our presently recorded uniaxial stress–strain curve until fracture thus constitute a comprehensive mechanical characterization, the finding on dramatically increasing Young's moduli are in accord with strongly increasing shear moduli determined in our previous shear rheology measurements on electron beam treated collagens of different source.[25] Clearly energetic electron assisted introduction of covalent crosslinks

constitutes the underlying mechanism. The latter is accomplished by a hydrolysis-based mechanism, *i.e.* secondary electrons generated by the primary 10 MeV primary electrons, primarily split water ($H_2O \rightarrow H^+ + OH^-$) (beyond chain scission to some minor extends). The resulting H^+ and OH^- radicals successively attack collagen side groups, resulting - as demonstrated by us for porcine/rat-tail collagen blends - primarily in biomimetic crosslinking *via* tropocollagen lysine side groups, while the backbone chains are kept intact.[32]

Clearly it is reasonable to assume, that the same energetic electron induced processes prevail also in presence of a prestress, *i.e.* crosslinks are expected to be introduced into the prestressed sample. However, the loci of the introduced crosslinks certainly will depend on the local network configuration, *viz.* local distances and displacement fields, which are related to global strains in a non-affine manner. Even though this relation certainly is expected to be complex, introduced covalent crosslinks certainly imprint (or, program) the local network configuration related to a global strain state - and then prevails even in absence of global stresses. Thus energetic electron
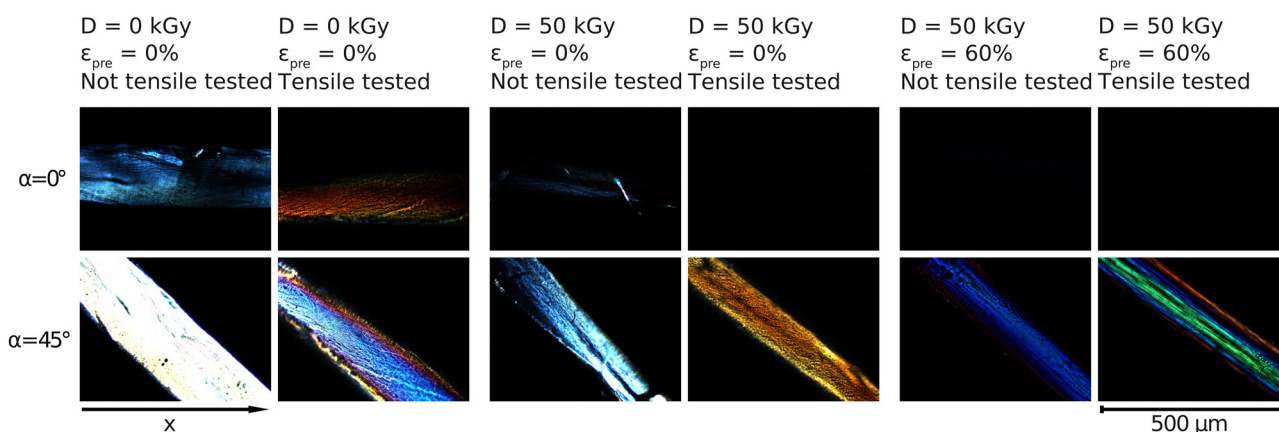

Fig. 5 Crossed polarized light microscopy measurements for samples with prestrains of ε_{pre} = 0% and ε_{pre} = 60% with regard to radiation treatment before and after tensile tests. The angle of the rotating plate in the polarization microscope is α. The microscopy images in higher resolution are shown in the Fig. S9–S13 (ESI†).
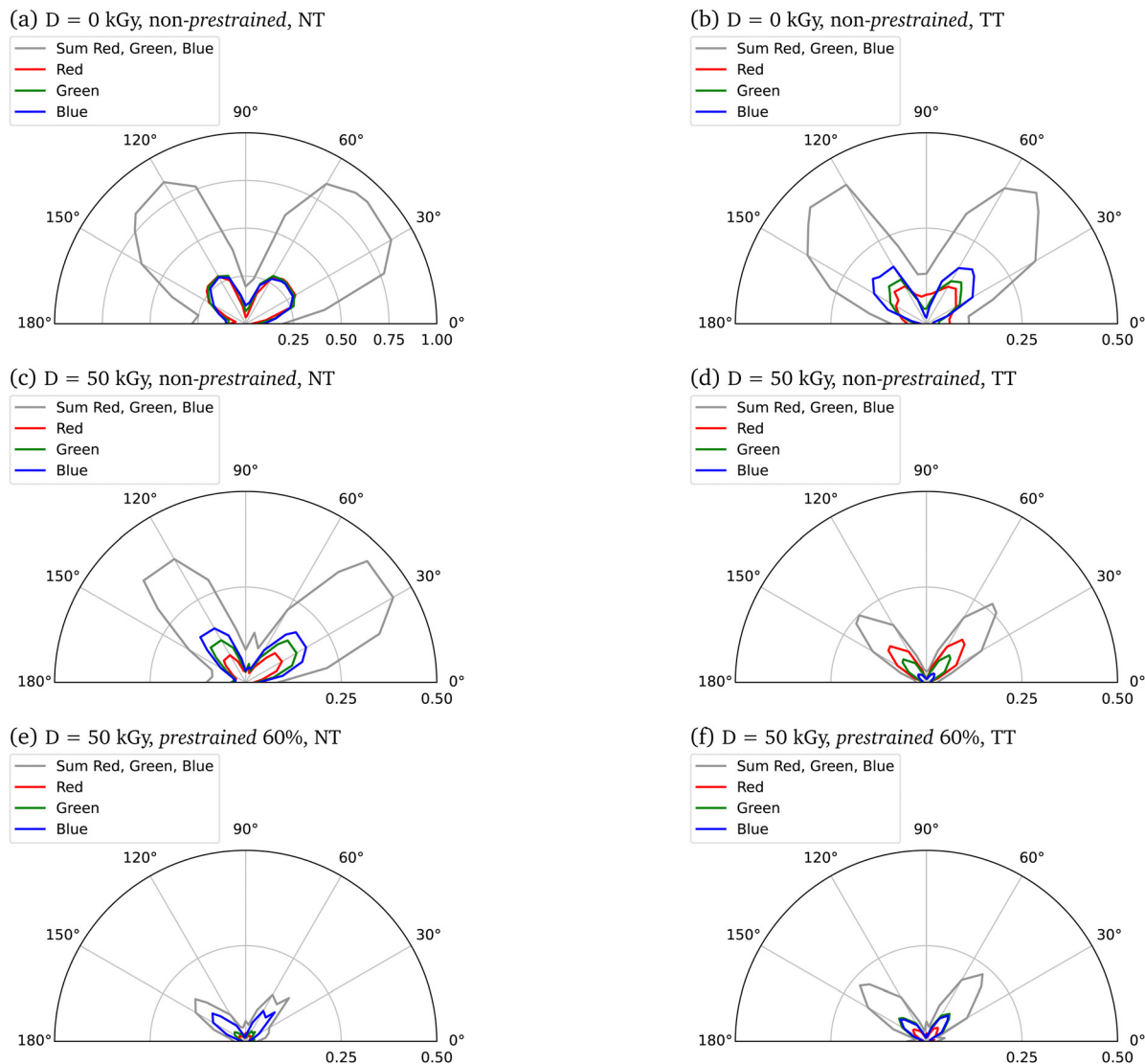
Fig. 6 Polar plots resulting from weighted mean intensities of the single red (R), green (G), blue (B) channels from individual pixel analysis of polarisation microscopy images. To obtain comparability at all rotation angles, the maximum circular area in the polarization microscopy images was considered. All areas outside the circle were set zero ($R = 0$, $G = 0$, $B = 0$). The lowest 5 intensities in the image matrix were weighted 0 in order to represent black (*i.e.* sample-free regions in the image, usually only the water) as little as possible in the polar plot. Shown are beside the mean R, G, B (weighted mean) intensities of the measurements also the summed intensities for all three channels together. Scaled are the means to the maximum possible intensity, both for *RGB* individually and for the sum of all *RGB* means. TT: tensile tested, NT: not tensile tested.

treatment at increasing strains is expected to result in increasingly unisotropic, covalently crosslinked collagen networks with fibers increasingly aligned along the prestraining direction.

This picture is, in fact, confirmed by our polarized light microscopy measurements (Fig. 5), that demonstrate an increased degree of axial fiber alignment for increasing prestrains and electron doses. Selective absorption or transmission of different wavelengths or polarizations of light at different orientations of the sample suggests the presence of optical phenomena called dichroism (Fig. 6). In parallel, these measurements indicate Mie and Rayleigh scattering due to the small-scale structures in collagen.[47–49] Several effects are to be expected that cause a change in the area under the curve due to a higher prestrain. Firstly, the geometric properties of the

sample are changed by the prestrain. Secondly, the morphology of the samples changes as a result of the prestrain. By increasing the anisotropy with an alignment of the internal collagen fibrils measured with polarization microscopy, a change in intensity can be observed. Polarization microscopy shows in particular the angle dependence of the intensity, which means that certain wavelengths are less intense depending on the angle. All colors must be considered when analyzing the alignment, as on the one hand a white light source with a non-monochromatic spectrum was used, and on the other hand scattering effects can occur in the material, which means that a certain wavelength does not locally characterize the material property at a certain point. The analysis here is qualitative, with a laser setup spatial heterogeneity of the material could be

analyzed even more precisely. Nevertheless, a higher angular dependence, *i.e.* a defined intensity maximum at a certain angle with a minimum curve width, can be used to interpret the measurements as a higher alignment of the collagen fibrils in the collagen fiber.

In a study by Cheung *et al.*,[50] radioactively labeled tissue treated by glutaraldehyde and a diamine crosslinking process was subcutaneously implanted in rats, whereby the amount of radioactivity remaining in the tissue, indicative of resistance to biodegradation, was monitored over a period of one year. The breakdown of a biomaterial *in vivo* is caused by either a chemical degradation or a mechanical wear-and-tear induced or enhanced by host immune response, calcification, specific cellular or enzymatic degradative processes.[50] In the case of a collagenous matrix, chemical degradation, namely proteolysis is the major cause of breakdown.[50] Although native helical collagen molecules and fibers are very resistant to proteases (except collagenases), any damage on any of the polypeptide chains within a molecule will cause the whole molecule to unwind and degrade quickly.[50] Mechanical stress or strain on the biopolymer *in vivo* may influence unwinding processes.[50] Crosslinks stabilize collagen as well as other macromolecules by allowing the partially cleaved peptides to remain folded in their native state.[50] Conversely, for long-term stability, the unwinding process of the collagen molecule, which in particular is (a) chemically or (b) mechanically induced, must be inhibited.

Concerning (a), native collagen generally has an isoelectric point near neutral pH, which means that it has poor water solubility under physiological conditions.[51] The pH and ionic strength of the suspending medium clearly affect the collagen solubility and also affect the relaxation of isometric forces caused by heating.[52] However, in collagenase solution the degree of enzymatic degradation of collagen hydrogels after immersion depends strongly on the crosslink density.[53] The resistance to collagenase of the cross-linked collagen hydrogels is greater than that of the native hydrogel.[53] This could be explained by the structural changes induced by cross-linking bonds.[53,54] Brodsky *et al.*[53,55] reported that the degradation was initiated by the cleavage of peptide bond at the site between residues 775 and 776 (Gly-Leu) in collagen triple helical domain due to collagenase. The fibrillar structure of collagen hydrogel became more compact *via* cross-linking and this steric hindrance decelerated the enzymatic degradation due to the inhibition of diffusion of collagenase to the cleavage sites.[53,56,57] As demonstrated by us,[32] at moderate doses crosslinks introduced into collagen due to application of energetic electrons are very much similar to crosslinks introduced biochemically under physiological conditions. Due to this biomimicry, we expect live expectancy of our crosslinks to be comparable to those introduced *in vivo* if not exposed to solubilizing enzymes or acidic conditions as mentionend above.

Regarding (b), a mechanically induced degradation of high-energy electron beam cross-linked collagen fibers, we refer to the relaxation analyses of the cyclic tests. Extrapolation of the fitted relaxation curves on more than 30 days using the optimised parameters from the adapted KWW function leads to stresses above 0.04 MPa and 0.22 MPa for 5 kGy without prestrain and for 5 kGy with 60% prestrain, respectively, being in the same order of magnitude and close to the stress of the first cycle in the respective loop of the measurement. Thus, the extrapolated data of the stretched exponential fit do not contradict long-term stability under repetitive load in an aqueous solution. However, the above-mentioned chemical effects can influence the morphology of the collagen fibres under permanent load in parallel to the mechanical degradation. Further experimental investigations under varying physiologically relevant conditions are required on the collagen system investigated here to monitor phenomena affecting the cross-link structure.

In terms of mechanics, it is noteworthy that our as-extruded collagen networks are largely isotropic subisostatic networks, whose mechanical response is established to be largely dominated by network topology and flexural moduli of fibers composing the network. With increased axial fiber alignment, uniaxial mechanical response is expected to be increasingly governed by axial Young's moduli of individual collagen fibers. In our mechanical measurement this scenario is, in fact, observed *e.g.* by an increase of the maximum Young's modulus by more than one order of magnitude when applying prestrain during exposure to an electron dose of 25 or 50 kGy (Fig. 1). Transition from a subisostatic random network to aligned fibers is also reflected by hysteresis, *viz.* energy dissipation. While it is established that subistostatic random networks (as the one obtained by our initial extrusion process) contain a large amount of floppy modes that dissipate energy during cycling, the latter are increasingly removed due to prestrain and electron induced crosslinking, *viz.* degeneracy regarding floppy modes is successively reduced. Within our cyclic mechanical tests this is reflected by a reduction of energy dissipation upon measuring cyclically, or, reduced broadness of hysteresis, or, equivalently, reduced imaginary part of the complex Young's modulus (Fig. 3).

Long-term swelling tests with collagen fibers were not carried out, although based on our previous work we expect a Flory–Rehner type of swelling behavior, in which osmotic pressure is balanced by network stresses, which, however, are generrated largely not entropically as in the original work, but by the more complex mechanical response of our electron beam crosslinked semiflexible collagen network, leading to reduced swelling with increasing mechanical stiffness. The collagen fibres were crosslinked in the fully hydraded state, whereby no instabilities were observed. Furthermore, the mechanical measurements of crosslinked fibers were also performed in the fully hydrated state after a swelling in distilled water, whereby no signs of disintegration were observed. However, studies have shown that collagen can denature in water at temperatures of around 80 °C, regardless of possible crosslinking techniques.[58] Our experiments were carried out at room temperature; the temperature was only exceeded during synthesis in a buffer at 36 °C and during irradiation, where local temperature peaks can occur. It is known that high temperatures in particular can have an influence on the denaturation of collagen.[59] It is therefore to be expected that at

temperatures higher than body temperature and high hydration states, the material properties may change, which could be investigated in detail in further long-term studies.

Regarding cell tests, our research group has carried out comprehensive studies on collagen scaffolds crosslinked with high-energy electrons. High cell viability and exceptional biocompatibility were observed even after modification with electron beams.[25] Compared to chemical crosslinking methods, no cytotoxic by-products are to be expected and thus an improvement in cell concerning properties. Further studies might provide a deeper understanding of collagen-cell interactions and thus future experiments need to be conducted.

Above, we have established a picture on how energetic electrons efficiently crosslink collagen and how this can be utilized to fixate fiber alignment with the help of prestrains. Despite preferential crosslinking sites *via* lysine side groups, energetic electron induced crosslinking remains a largely stochastic process regarding spatial distribution of the resulting crosslinks. These inherent spatial fluctuations in crosslink distributions will certainly lead to fluctuations in the energetics of activated processes, *viz.* increase temporal heterogeneity in thermally activated processes due to spatial heterogeneities. Generally, increasing presence of heterogeneities is reflected by increasing streched exponential relaxation behavior, *i.e.* increasing deviation of the Kohlrausch exponent $\beta \leq 1$ from $\beta = 1$ (eqn (2)). In fact, upon increasing electron dose, decreasing Kohlrausch exponents β are observed, consistent with this interpretation (Fig. 4).

In short term, applications as suture in medical surgeries seem in reach. In the long term, the synthesis of artificial tendons or ligaments clearly is a vision. However, as the mechanical response in tendons and ligaments is governed by the complex hierarchical collagen structure, further structural tuning employing several steps in synthesis and radiation gradients will be key aspects to come closer to mimic biological response.

5 Conclusion

Within the present work we have demonstrated how application of mechanical strains during energetic electron assisted crosslinking of collagen can be employed to design anisotropic fibers with variable degree of axial network fiber alignment. While we have verified that programming of fiber alignment is feasible with this approach using polarized light microscopy, it allows for the design of highly customized collagen fibers with tailorable anisotropy and mechanical properties. Our presently reported finding thus paves the way for synthesizing advanced biomimetic scaffolds of highly variable anisotropy and mechanical response, potentially suitable for a broad range of applications in biomedicine.

6 List of abbreviations

| PLM | Polarized light microscopy |
| FFB | Fiber formation buffer |

PTFE	Polytetrafluoroethylene
LED	Light-emitting diode
UTS	Ultimate tensile strength
LED	Light-emitting diode
KWW	Kohlrausch–Williams–Watt function
RGB	RGB color model
ESEM	Environmental scanning electron microscope

Availability of data and materials

The datasets used and/or analyzed during the current study are available from the corresponding authors on reasonable request.

Authors' contributions

Anastassiya Bublikova: investigation, conceptualization, data curation, methodology, visualization, writing – original draft, writing – review & editing. Friedrich Schütte: conceptualization, methodology, supervision, visualization, writing contribution to the original draft, writing – review & editing. Stefan G. Mayr: project idea, funding acquisition, supervision, project administration, writing – review & editing. Anastassiya Bublikova and Friedrich Schütte contributed equally to this work. All authors read and approved the final manuscript.

Conflicts of interest

The authors declare that they have no known competing financial interests or personal relationships that could have appeared to influence the work reported in this paper.

Acknowledgements

Notes and references

1 M. C. Catoira, L. Fusaro, D. Di Francesco, M. Ramella and F. Boccafoschi, *J. Mater. Sci.: Mater. Med.*, 2019, **30**, 115.

2 C. Frantz, K. M. Stewart and V. M. Weaver, *J. Cell Sci.*, 2010, **123**, 4195–4200.

3 J. A. Ramshaw, P. R. Vaughan and J. A. Werkmeister, *Biomed. Eng.*, 2001, **13**, 14–26.

4 T. Rozario and D. W. DeSimone, *Dev. Biol.*, 2010, **341**, 126–140.

5 M. Shoulders and R. Raines, *Annu. Rev. Biochem.*, 2009, **78**, 929–958.

6 S. A. Sell, P. S. Wolfe, K. Garg, J. M. McCool, I. A. Rodriguez and G. L. Bowlin, *Polymers*, 2010, **2**, 522–553.

7 K. E. Kadler, C. Baldock, J. Bella and R. P. Boot-Handford, *J. Cell Sci.*, 2007, **120**, 1955–1958.

8 J. Lin, Y. Shi, Y. Men, X. Wang, J. Ye and C. Zhang, *Tissue Eng., Part B*, 2020, **26**, 116–128.

9 K. Gelse, E. Pöschl and T. Aigner, *Adv. Drug Delivery Rev.*, 2003, **55**, 1531–1546.

10 C. Söderhäll, I. Marenholz, T. Kerscher, F. Rüschendorf, J. Esparza-Gordillo, M. Worm, C. Gruber, G. Mayr, M. Albrecht, K. Rohde, H. Schulz, U. Wahn, N. Hubner and Y.-A. Lee, *PLoS Biol.*, 2007, **5**, 1–10.

11 S. H. Liu, R.-S. Yang, R. Al-Shaikh and J. M. Lane, *Clin. Orthop. Relat. Res.*, 1995, **318**, 265–278.

12 C. Lovell, K. Smolenski, V. Duance, N. Light, S. Young and M. Dyson, *Br. J. Dermatol.*, 1987, **117**, 419–428.

13 S. Münster, L. M. Jawerth, B. A. Leslie, J. I. Weitz, B. Fabry and D. A. Weitz, *Proc. Natl. Acad. Sci. U. S. A.*, 2013, **110**, 12197–12202.

14 B. A. Roeder, K. Kokini, J. E. Sturgis, J. P. Robinson and S. L. Voytik-Harbin, *J. Biomech. Eng.*, 2002, **124**, 214–222.

15 C. Storm, J. J. Pastore, F. C. MacKintosh, T. C. Lubensky and P. A. Janmey, *Nature*, 2005, **435**, 191–194.

16 D. M. Knapp, V. H. Barocas, A. G. Moon, K. Yoo, L. R. Petzold and R. T. Tranquillo, *J. Rheol.*, 1997, **41**, 971–993.

17 S. Noorzai, C. J. R. Verbeek, M. C. Lay and J. Swan, *Waste Biomass Valorization*, 2020, **11**, 5687–5698.

18 J. Chen, K. Gao, S. Liu, S. Wang, J. Elango, B. Bao, J. Dong, N. Liu and W. Wu, *Mar. Drugs*, 2019, **17**, 33.

19 Y. Kato, D. L. Christiansen, R. A. Hahn, S.-J. Shieh, J. D. Goldstein and F. H. Silver, *Biomaterials*, 1989, **10**, 38–42.

20 W. Liu, K. Merrett, M. Griffith, P. Fagerholm, S. Dravida, B. Heyne, J. C. Scaiano, M. A. Watsky, N. Shinozaki, N. Lagali, R. Munger and F. Li, *Biomaterials*, 2008, **29**, 1147–1158.

21 V. Chak, D. Kumar and S. Visht, *Int. J. Pharm. Teach. Pract.*, 2013, **4**, 811–820.

22 Y. Zhang, Y. Wang, Y. Li, Y. Yang, M. Jin, X. Lin, Z. Zhuang, K. Guo, T. Zhang and W. Tan, *Gels*, 2023, **9**, 185.

23 G. Liu, R. Agarwal, K. Ko, M. Ruthven, H. Sarhan and J. Frampton, *Sci. Rep.*, 2017, **7**, 9628.

24 L. Fan, Y. Ren, S. Emmert, I. Vučković, S. Stojanovic, S. Najman, R. Schnettler, M. Barbeck, K. Schenke-Layland and X. Xiong, *Int. J. Mol. Sci.*, 2023, **24**, 3744.

25 S. Riedel, P. Hietschold, C. Krömmelbein, T. Kunschmann, R. Konieczny, W. Knolle, C. T. Mierke, M. Zink and S. G. Mayr, *Mater. Des.*, 2019, **168**, 107606.

26 N. E. Ben Ammar, T. Saied, M. Barbouche, F. Hosni, M. Adel and M. Sen, *Polym. Bull.*, 2018, **75**, 3825–3841.

27 I. Sallent, H. Capella and D. Zeugolis, *Production and Characterization of Chemically Cross-Linked Collagen Scaffolds: Methods and Protocols*, Springer, 2019, vol. 1944, pp. 23–38.

28 M. Nair, S. M. Best and R. E. Cameron, *Appl. Sci.*, 2020, **10**, 6911.

29 A. Bigi, G. Cojazzi, S. Panzavolta, K. Rubini and N. Roveri, *Biomaterials*, 2001, **22**, 763–768.

30 D. P. Speer, M. Chvapil, C. D. Eskelson and J. B. Ulreich, *J. Biomed. Mater. Res.*, 1980, **14**(6), 753–764.

31 J. E. Gough, C. A. Scotchford and S. Downes, *J. Biomed. Mater. Res.*, 2002, **61**, 121–130.

32 N. Wilharm, M. Bertmer, W. Knolle, J. Griebel, C. Elsner and S. G. Mayr, *Acta Biomater.*, 2022, **140**, 219–232.

33 S. Riedel, K. Bela, E. I. Wisotzki, C. Suckfull, J. Zajadacz and S. G. Mayr, *Mater. Design*, 2018, **153**, 80–85.

34 E. I. Wisotzki, M. Hennes, C. Schuldt, F. Engert, W. Knolle, U. Decker, J. A. Käs, M. Zink and S. G. Mayr, *J. Mater. Chem. B*, 2014, **2**, 4297–4309.

35 J. A. Paten, S. M. Siadat, M. E. Susilo, E. N. Ismail, J. L. Stoner, J. P. Rothstein and J. W. Ruberti, *ACS Nano*, 2016, **10**, 5027–5040.

36 C. Guo and L. J. Kaufman, *Biomaterials*, 2007, **28**, 1105–1114.

37 Y. Eguchi, S. Ohtori, M. Sekino and S. Ueno, *Bioelectromagnetics*, 2015, **36**, 233–243.

38 C. Chaubaroux, F. Perrin-Schmitt, B. Senger, L. Vidal, J.-C. Voegel, P. Schaaf, Y. Haikel, F. Boulmedais, P. Lavalle and J. Hemmerlé, *Tissue Eng., Part C*, 2015, **21**, 881–888.

39 D. Vader, A. Kabla, D. Weitz and L. Mahadevan, *PLoS One*, 2009, **4**, e5902.

40 R. Oldenbourg, *Cold Spring Harbor Protocols*, 2013, **2013**, pdb.top078600.

41 Leica DM2700 M Instructions.

42 T. Golde, M. Glaser, C. Tutmarc, I. Elbalasy, C. Huster, G. Busteros, D. M. Smith, H. Herrmann, J. A. Käs and J. Schnauß, *Soft Matter*, 2019, **15**, 4865–4872.

43 G. Van Rossum and F. L. Drake, *Python 3 Reference Manual, CreateSpace*, Scotts, Valley, CA, 2009.

44 R. June, C. Neu, J. R. Barone and D. Fyhrie, *Mater. Sci. Eng., C*, 2011, **31**, 781–788.

45 R. K. June and D. P. Fyhrie, *Comput. Methods Biomech. Biomed. Eng.*, 2013, **16**, 565–576.

46 F. Schütte and S. Mayr, *ACS Biomater. Sci. Eng.*, 2024, **10**(2), 782–790.

47 S. L. Jacques, *Adv. Opt. Imaging Photon Migr.*, 1996, OPC364.

48 A. P. M. Michel, S. Liakat, K. Bors and C. F. Gmachl, *Biomed. Opt. Express*, 2013, **4**, 520–530.

49 Z. Gajinov, M. Matić, S. Prćić and V. Duran, *Serbian J. Dermatology Venereol*, 2013, **2**, 131–136.

50 D. T. Cheung, D. Tong, N. Perelman, D. Ertl and M. E. Nimni, *Connect. Tissue Res.*, 1990, **25**, 27–34.

51 Y. Junhui, C. Ding, L. Tang, F. Deng, Y. Qili, H. Wu, L. Chen, Y. Ni, L. Huang and M. Zhang, *ACS Omega*, 2020, **5**(11), 5772–5780.

52 M. E. Latorre, A. L. Lifschitz and P. P. Purslow, *Meat Sci.*, 2016, **118**, 78–81.

53 Z. Tian, W. Liu and G. Li, *Polym. Degrad. Stab.*, 2016, **130**, 264–270.

54 S. Park, J. Park, H. Kim, M. Song and H. Suh, *Biomaterials*, 2002, **23**, 1205–1212.

55 B. Brodsky and J. A. Ramshaw, *Matrix Biol.*, 1997, **15**, 545–554.

56 H. Saito, T. Taguchi, H. Kobayashi, K. Kataoka, J. Tanaka, S. Murabayashi and Y. Mitamura, *Mater. Sci. Eng. C*, 2004, **24**, 781–785.

57 D. P. Speer, M. Chvapil, C. D. Eskelson and J. B. Ulreich, *J. Biomed. Mater. Res.*, 1980, **14**(6), 753–764.

58 Y. Suwa, K. Nam, K. Ozeki, T. Kimura, A. Kishida and T. Masuzawa, *J. Biomed. Mater. Res., Part B*, 2016, **104**, 538–545.

59 L. Bozec and M. Odlyha, *Biophys. J.*, 2011, **101**, 228–236.